

# Highly Variable $\gamma$ -Ray Emission of CTD 135 and Implications for its Compact Symmetric Structure

Ying-Ying Gan<sup>1</sup>, Hai-Ming Zhang<sup>2</sup>, Jin Zhang<sup>3†</sup>, Xing Yang<sup>1</sup>, Ting-Feng Yi<sup>4</sup>, Yun-Feng Liang<sup>1</sup> and En-Wei Liang<sup>1</sup>

<sup>1</sup> Guangxi Key Laboratory for Relativistic Astrophysics, School of Physical Science and Technology, Guangxi University, Nanning 530004, People's Republic of China

<sup>2</sup> School of Astronomy and Space Science, Nanjing University, Nanjing 210023, People's Republic of China

<sup>3</sup> School of Physics, Beijing Institute of Technology, Beijing 100081, People's Republic of China; j.zhang@bit.edu.cn

<sup>4</sup> Department of Physics, Yunnan Normal University, Kunming 650500, People's Republic of China

**Abstract** The  $\gamma$ -ray emission properties of CTD 135, a typical compact symmetric object (CSO), are investigated with  $\sim 11$ -year Fermi/LAT observations. We show that it has bright and significantly variable GeV emission, with the  $\gamma$ -ray luminosity of  $L_\gamma \sim 10^{47}$  erg s<sup>-1</sup> and a variation index of  $TS_{\text{var}} = 1002$ . A quasi-periodic oscillation (QPO) with a periodicity of  $\sim 460$  days is detected in the global 95% false-alarm level. These  $\gamma$ -ray emission features are similar to that of blazars. Its broadband spectral energy distribution (SED) can be attributed to the radiations of the relativistic electrons accelerated in the core region and the extended region. The SED modeling shows that the  $\gamma$ -rays are from the core region, which has a Doppler boosting factor of  $\delta \sim 10.8$  and relativistically moves with a small viewing angle, being similar to blazar jets. On the base of the analysis results, we propose that the episodic activity of the central engine in CTD 135 results in a blazar-like jet and the bubble-like lobes as the Fermi bubbles in the Galaxy. The strong  $\gamma$ -ray emission with obvious variability is from the jet radiations and the symmetric radio structure is attributed to the bubbles. The jet radiation power and disk luminosity in units of Eddington luminosity of CTD 135 follow the same relation as other young radio galaxies, indicating that its jet radiation may be also driven by the Eddington ratio.

**Key words:** galaxies: active—galaxies: jets—radio continuum: galaxies—gamma rays:

## 1 INTRODUCTION

Compact symmetric objects (CSOs) are of a sub-class of misaligned active galactic nuclei (AGNs), being characterized by a symmetric and sub-kiloparsec (sub-kpc) radio structure (Phillips & Mutel 1980; Wilkinson et al. 1994; Readhead et al. 1996a). The radio spectra of some CSOs exhibit a turnover around a few GHz frequency (de Vries et al. 1997; Murgia 2003), similar to gigahertz peaked-spectrum sources (GPSs, O’Dea 1998; Fanti 2009). The radio emission of CSOs displays weak variability (Fassnacht & Taylor 2001) and low polarization (Peck & Taylor 2000). Although they may also be confined to the sub-kpc scale by a dense and turbulent ambient medium (van Breugel et al. 1984; O’Dea 1998), it is still lack of observational evidence that the amount of ambient gas can supply enough confinement. They are generally thought as young radio galaxies and the progenitors of the extended radio galaxies (e.g., Phillips & Mutel 1982; Fanti et al. 1995; Readhead et al. 1996b). However, only a fraction of CSOs may evolve into large-scale radio galaxies (An & Baan 2012). The radio luminosity would decrease by an order of magnitude as the radio size of source grows from a few kpc to hundreds of kpc (Fanti et al. 1995; Begelman 1996; Readhead et al. 1996a,b), and the compact sources will evolve into objects less powerful than the most powerful classical doubles (O’Dea & Baum 1997; Stanghellini et al. 1998). As representatives of young AGNs, CSOs are of interest for understanding the early evolution and the jet radiation physics of AGNs.

Strong  $\gamma$ -ray emission from the parsec-scale (pc-scale) lobes of young radio sources was theoretically predicted (Stawarz et al. 2008; Kino et al. 2007, 2009; Kino & Asano 2011; Migliori et al. 2014), but systematic search for CSOs in the  $\gamma$ -ray band is rather unsuccessful (D’Ammando et al. 2016). So far, only a few CSOs were detected in the  $\gamma$ -ray band, including PMN J1603–4904 (Müller et al. 2014, 2015), PKS 1718–649 (Migliori et al. 2016), NGC 3894 (Principe et al. 2020), and TXS 0128+554 (Lister et al. 2020). The origin of  $\gamma$ -ray emission in CSOs is still debated. The  $\gamma$ -ray emission of TXS 0128+554 likely originates in the inner jet/core region since the predicted flux by the inverse Compton emitting cocoon model is seriously lower than the observed Fermi/LAT flux (Lister et al. 2020). Thus, the  $\gamma$ -rays in these CSOs may indicate a hallmark of recently restarted jet activity (Lister et al. 2020). By studying the  $\gamma$ -ray emission in radio galaxies with the very long baseline interferometry (VLBI), Angioni et al. (2020) suggested that the high-energy emission of radio galaxies is related to the pc-scale radio emission from the inner jet, but the  $\gamma$ -ray loudness does not be connected with a higher prevalence of Doppler boosting effect (see also Angioni et al. 2019). The asymmetric jets seen in some CSOs might be evidence for bulk relativistic motion (Readhead et al. 1996b). CSOs with a visibly detected core, especially accompanying variability, also likely indicate the Doppler boosting effect in these core regions (Peck & Taylor 2000; Gugliucci et al. 2005).

CTD 135 (also named as 2234+282) is a CSO located at a redshift of  $z = 0.795$  (Schmidt 1977). With the very large array (VLA) observation at 1.64 GHz, Murphy et al. (1993) revealed a bright compact component and a weak feature separated about  $4.''9$  and reported that CTD 135 is a powerful core-dominated radio source. However, the very long baseline array (VLBA) images at 2.3 GHz show as a single compact component, which is well resolved along the northeast-southwest direction at 8.4 GHz and 15 GHz (An et al. 2016). It exhibits a compact triple structure at 15 GHz with a likely core between component-

2016). In this paper, we focus on its properties of  $\gamma$ -rays observed with the Fermi/LAT in order to reveal the radiation physics and the nature of its symmetric radio structure.

## 2 FERMI/LAT DATA REDUCTION AND ANALYSIS

Fermi/LAT is a  $\gamma$ -ray telescope covering a wide energy range from 20 MeV to more than 300 GeV. It is a powerful tool for monitoring  $\gamma$ -ray emission from AGNs. Fermi/LAT Pass 8 data, which approximately covers  $\sim 11$ -year (MET 239557417–584235367), is used in our analysis. We only focus on photons within the  $15^\circ$  region of interest (ROI) centered on the radio position of CTD 135 (R.A. = 339.094, Decl. = 28.483; Johnston et al. 1995). We select the  $\gamma$ -ray events in the energy range of 0.1–300 GeV, using standard data quality selection criteria “(DATA\_QUAL>0)&&(LAT\_CONFIG==1)”. The maximum zenith angle of  $90^\circ$  is set to reduce the  $\gamma$ -ray contamination from the Earth limb. The P8R3\_SOURCE\_V2 set of instrument response function and the publicly available software *fermitools* (ver. 1.0.0) with the binned likelihood analysis method is used in our data analysis.

We employ the maximum test statistic (TS) to identify a point source from the background, where  $TS = 2\log(\frac{\mathcal{L}_{src}}{\mathcal{L}_{null}})$ , i.e., the logarithmic ratio of the likelihood for a model with the point source to a model without the point source (Mattox et al. 1996). A source with a maximum likelihood  $TS > 25$  is considered as a point source (Abdollahi et al. 2020). The background model includes the isotropic emission (i.e., iso\_P8R3\_SOURCE\_V2\_v1.txt) and the diffuse Galactic interstellar emission (i.e., gll\_iem\_v07.fits), as well as all the  $\gamma$ -ray sources listed in the Fourth Fermi LAT Source Catalog (4FGL, Abdollahi et al. 2020). We keep the normalization of the isotropic emission and the diffuse Galactic interstellar emission free. The normalization and spectral parameters of the  $\gamma$ -ray sources within  $10^\circ$  in the background model were set to be free. In 4FGL (Abdollahi et al. 2020), the  $\gamma$ -ray source 4FGL J2236.3+2828 was reported to be associated with CTD 135 (see also An et al. 2016). Note that the  $\sim 11$ -year Pass 8 data is used in our analysis, but the 4FGL was extracted with the 8-year Fermi/LAT observation data. We firstly make a test of new point sources in the 11-year Fermi/LAT data. After subtracting all the background models, we find that the maximum value in the residual TS map is 7.5, excluding the possibility of new point sources in the 11-year data. Our result is shown in Figure 1, confirming that CTD 135 is spatially associated with 4FGL J2236.3+2828.

The “LogParabole” spectral model is adopted in our analysis for 4FGL J2236.3+2828, i.e.,

$$\frac{dN}{dE} = N_0 \left(\frac{E}{E_b}\right)^{-(\Gamma_\gamma + \beta \log(\frac{E}{E_b}))}, \quad (1)$$

where  $E_b$  is the reference energy,  $\Gamma_\gamma$  is the photon spectral index and  $\beta$  is the curvature (Massaro et al. 2004). This model is typically used to describe the spectra of blazars in 4FGL. The curvature of a spectrum is evaluated with  $TS_{curv} = 2\log(\mathcal{L}_{LP}/\mathcal{L}_{PL})$ , where  $\mathcal{L}_{LP}$  and  $\mathcal{L}_{PL}$  are the likelihoods of hypothesis for testing LogParabole model and power-law model, respectively. In case of  $TS_{curv} > 9$ , the curvature of a spectrum is significant at  $\sim 3\sigma$  confidence level (Abdollahi et al. 2020). The derived  $TS_{curv}$  is 90 for 4FGL J2236.3+2828, implying that its spectrum is significantly curved. As shown in Figure 2, the spectral shape of 4FGL J2236.3+2828 can be well fit by the “LogParabole” spectral model. The best-fit results are  $\Gamma_\gamma = 2.137 \pm 0.001$ ,  $\beta = 0.079 \pm 0.001$ , and  $E_b = 548.34$  MeV with  $TS = 12558$ . The derived average

We extract the long-term light curve of CTD 135 by adopting a criterion of  $TS > 25$  for each time interval and a minimum time-bin of 7 days. Our results are shown in Figure 2. The likelihood-based statistic method is most commonly used to quantify the variability of sources (Nolan et al. 2012; Peng et al. 2019; Abdollahi et al. 2020; Xi et al. 2020). We evaluate the variability of the  $\gamma$ -ray emission for CTD 135 with an index of  $TS_{\text{var}}$  as defined in Nolan et al. (2012), and obtain  $TS_{\text{var}} = 1002$  for CTD 135. Note that if  $TS_{\text{var}} > 25.4$ , the confidence level of the variability is  $3\sigma$  in a  $\chi^2_{N-1}(TS_{\text{var}})$  distribution with  $N - 1 = 9$  degrees of freedom, and  $N$  is the number of time-bins. Therefore, CTD 135 is an extremely variable source in the  $\gamma$ -ray band.

Inspecting the long-term  $\gamma$ -ray light curve of CTD 135, one can observe a tentative quasi-periodic oscillation (QPO) signature. We analyze the power density spectrum (PDS) of the  $\gamma$ -ray light curve and evaluate the QPO signature with the Lomb–Scargle Periodogram (LSP) algorithm (Lomb 1976; Scargle 1982; see Zhang et al. 2017 for more detail). The PDS is presented in figure 3, which shows a visible peak at  $\sim 460$  days. The highest peak of PDS at  $\sim 460$  days is beyond the global 95% false-alarm level, likely indicating that a QPO signature is presented in the  $\gamma$ -ray light curve of CTD 135.

### 3 BROADBAND SED CONSTRUCTING AND MODELING

Using the  $\gamma$ -ray data derived above together with the other multi-wavelength data collected from the ASI Science Data Center (ASDC) and the NASA/IPAC Extragalactic Database (NED), we compile the broadband spectral energy distribution (SED) of CTD 135, as illustrated in Figure 4. The most striking feature of the SED is the triple peaks at the optical, X-ray and GeV  $\gamma$ -band bands. The broadband SEDs of the  $\gamma$ -ray emitting compact steep-spectrum sources (CSSs) can be well explained by the two-zone leptonic radiation model (Zhang et al. 2020a). Hence, we also consider the same model to fit the SED of CTD 135, i.e., the radiations of the relativistic electrons in both compact core and extended region (component-NE and component-SW), including the synchrotron (syn), synchrotron-self-Compton (SSC), and external Compton (EC) scattering of the relativistic electrons. The electron energy distributions in the range of  $[\gamma_{\text{min}}, \gamma_{\text{max}}]$  for both the core and extended regions are taken as a broken power-law with indices  $p_1$  and  $p_2$  as well as a break at  $\gamma_b$ , i.e.,

$$N(\gamma) = N_0 \begin{cases} \gamma^{-p_1} & \gamma_{\text{min}} \leq \gamma \leq \gamma_b, \\ \gamma_b^{p_2-p_1} \gamma^{-p_2} & \gamma_b < \gamma < \gamma_{\text{max}}. \end{cases} \quad (2)$$

For the core region, the radiation region is assumed as a homogenous sphere with radius  $R$  and magnetic field strength  $B$ , where  $R$  is estimated with  $R = \delta c \Delta t / (1 + z)$ . Since the observed time-scale of  $\gamma$ -ray flux variation is smaller than 7 days (as displayed in Figure 2), we take  $\Delta t = 7$  days. The brightness temperature and variability of the radiations from the core region indicate its Doppler boosting effect (Hovatta et al. 2009; An et al. 2016; Lioudakis et al. 2018). We thus consider the relativistic motion of the core region with the bulk Lorentz factor  $\Gamma$  and the Doppler factor  $\delta$ . Since the  $\gamma$ -ray luminosity of CTD 135 is bright and variable as blazars, we fit the SED by assuming  $\delta = \Gamma$  as done for blazars (e.g., Zhang et al. 2012, 2015). The photon field from the outer region of broad line regions (BLRs) is used to calculate the EC process<sup>1</sup>.

<sup>1</sup> Since the radiation region is far away from the black hole and the accretion disk emission is not important anymore, we thus do

The minimum energy of the radiation electrons is fixed as  $\gamma_{\min} = 1$  and the maximum energy  $\gamma_{\max}$  is poorly constrained by the last observation point in the  $\gamma$ -ray band. Spectral indices  $p_1$  and  $p_2$  are taken the values derived from the observed SEDs.

For the extended region, the radiation region is also assumed as a homogenous sphere with an angular radius of 5 mas (approximate distance between component-NE and component-SW in An et al. 2016). The derived average hot-spot advance speed between component-NE and component-SW is  $\sim 0.3c$  (An et al. 2016). The symmetric radio structure may also imply a large viewing angle to the extended region, we thus do not consider the relativistic motion and the Doppler boosting effect. The contribution of the inverse Compton scattering of cosmic microwave background photons (IC/CMB) by the relativistic electrons is considered. The SED modeling for the extended region is under the equipartition condition, i.e., the energy densities of the magnetic fields ( $U_B$ ) and electrons ( $U_e$ ) are equal. We also set  $\gamma_{\min} = 1$  and  $\gamma_{\max} = 50*\gamma_b$ .  $p_1$  is fixed as the value derived by fitting the radio spectrum and  $p_2$  is fixed as  $p_2 = 4$ .

There are not enough simultaneous observational data to constrain the parameters as done for blazars in our previous works (e.g., Zhang et al. 2012, 2015), so the goodness of SED fitting is assessed visually. The synchrotron-self-absorption, the Klein–Nishina effect, and the absorption of high-energy  $\gamma$ -ray photons by extragalactic background light (Franceschini et al. 2008) are also taken into account. As illustrated in Figure 4, the model can well represent the SED. We obtain  $R = 1.1 \times 10^{17}$  cm,  $B = 0.97$  G,  $\delta = \Gamma = 10.8$ ,  $\gamma_b = 373$ ,  $\gamma_{\max} = 5500$ ,  $N_0 = 286.4 \text{ cm}^{-3}$ ,  $p_1 = 1.7$ ,  $p_2 = 3.76$ ,  $U_{\text{BLR}} = 1.1 \times 10^{-3} \text{ erg cm}^{-1}$  (energy density of the outer region for BLR) for the core region;  $R = 37.51$  pc,  $B_{\text{eq}} = 8.57$  mG,  $\gamma_b = 2200$ ,  $N_0 = 0.012 \text{ cm}^{-3}$ , and  $p_1 = 1.35$  for the extended region, respectively. It is found that the  $\gamma$ -rays are contributed by the EC/BLR process, the X-ray emission is dominated by the SSC process of the core region, and the IR-optical bump is attributed to the synchrotron emission of the electrons in the core region. Although the electrons in the extended region are more energetic than that in the core region, their synchrotron radiations peak at  $10^{10}$  Hz since the magnetic field strength of the extended region is much lower than that of the core region. The radiations from the SSC process of both the core and extended regions peak at a similar frequency range. And the emission of the IC/CMB process from the extended region also peaks at the same range, but its flux is extremely low.

We obtain  $\delta = 10.8$  for the core region, which is larger than the variability Doppler factor of  $\delta_{\text{var}} = 6$  inferred by the flux-density variations at the radio band in Hovatta et al. (2009), but smaller than the reported value of  $\delta_{\text{var}} = 20.19$  in Liodakis et al. (2018). Both CSOs and CSSs belong to young radio-loud AGNs. As displayed in Figure 5, the core region of CTD 135 has the larger  $B$  and  $\delta$ , on average smaller  $\gamma_b$  than those of  $\gamma$ -ray emitting CSSs (the data of CSSs to see Zhang et al. 2020a), indicating that the stronger radiation cooling for the electrons by the magnetic field and EC process in CTD 135 than in those CSSs. Similar to the  $\gamma$ -ray emitting CSSs,  $p_1 = 1.7$  is smaller than the expected value of 2 from the shock acceleration mechanism (e.g., Kirk et al. 2000; Achterberg et al. 2001; Virtanen & Vainio 2005). The flatter power-law particle spectrum may be due to the magnetic reconnection acceleration process (Zenitani & Hoshino 2001; Sironi & Spitkovsky 2014; Guo et al. 2015; Zhu et al. 2016). For the extended region, the derived equipartition magnetic field of  $B_{\text{eq}} = 8.57$  mG is comparable to the typical range of

## 4 DISCUSSION

### 4.1 Powers of the Core Region in Comparison with $\gamma$ -ray Emitting CSOs and CSSs as well as Blazars

CSOs may evolve first into CSSs and then into FR II radio galaxies (Readhead et al. 1996a). As displayed in Figure 6, CTD 135 is the brightest one among the  $\gamma$ -ray selected CSOs and CSSs. The  $\sim 11$ -year average luminosity of CTD 135 is  $L_\gamma \sim 10^{47}$  erg s $^{-1}$ , and  $L_\gamma$  is almost close to  $10^{48}$  erg s $^{-1}$  in some time-bins as shown in Figure 2. As reported in Abdollahi et al. (2020; see also Lister et al. 2020), NGC 3894 is the lowest luminosity CSO with  $L_\gamma < 10^{42}$  erg s $^{-1}$  and a flat photon index of  $2.06 \pm 0.12$ ; PKS 1718–649 also has a low luminosity ( $L_\gamma \sim 10^{42.1}$  erg s $^{-1}$ ), but has a steeper photon index of  $2.49 \pm 0.18$  than NGC 3894; both TXS 0128+554 and PMN 1603–4904 have the flat photon index similar to NGC 3894 with the higher luminosity ( $10^{43} < L_\gamma < 10^{46}$  erg s $^{-1}$ ). Different from CTD 135, the four  $\gamma$ -ray emitting CSOs do not show fast and obvious variabilities at the  $\gamma$ -ray band.  $L_\gamma$  of CTD 135 is similar to some bright flat-spectrum radio quasars (FSRQs, a sub-class of blazars). The derived values of  $B$ ,  $\delta$ , and  $\gamma_b$  are also similar to those of blazars (Zhang et al. 2012, 2015).

On the basis of the SED fitting parameters, we calculate the jet powers in case of the  $e^\pm$  pair jet for the core region of CTD 135. The powers of radiation electrons ( $P_e$ ) and magnetic fields ( $P_B$ ) are calculated by  $P_i = \pi R^2 \Gamma^2 c U_i$ , where  $U_i$  is  $U_e$  or  $U_B$ . The radiation power is  $P_r = \pi R^2 \Gamma^2 c U_r = L_{\text{bol}} \Gamma^2 / 4 \delta^4$ , where  $L_{\text{bol}}$  is the non-thermal radiation luminosity of the core region. We obtain  $P_e = 6.03 \times 10^{44}$  erg s $^{-1}$ ,  $P_B = 4.89 \times 10^{45}$  erg s $^{-1}$ ,  $P_r = 7.29 \times 10^{44}$  erg s $^{-1}$ , and  $P_{\text{jet}}^{e^\pm} = P_e + P_B + P_r = 6.23 \times 10^{45}$  erg s $^{-1}$ . We also obtain  $P_r / P_{\text{jet}}^{e^\pm} = 0.12$  and  $P_B / P_{\text{jet}}^{e^\pm} = 0.79$ , indicating that the core region of CTD 135 may be highly magnetized with high radiation efficiency, similar to FSRQs and narrow-line Seyfert 1 galaxies (NLS1s) as well as  $\gamma$ -ray emitting CSSs (Zhang et al. 2014, 2015, 2020a; Sun et al. 2015).

As shown in Figure 4, no apparent thermal-radiation component from the accretion disk is observed in the broadband SED of CTD 135. If the disk luminosity ( $L_{\text{disk}}$ ) of CTD 135 is estimated by  $L_{\text{disk}} = 10 * L_{\text{BLR}}$ , where  $L_{\text{BLR}}$  is the BLR luminosity and taken from Celotti et al. (1997), we obtain  $L_{\text{disk}} \sim 6.03 \times 10^{45}$  erg s $^{-1}$ . The central black hole mass is  $M_{\text{BH}} = 10^{8.35} M_\odot$  (Shaw et al. 2012), hence the derived Eddington-ratio ( $R_{\text{Edd}}$ ) of CTD 135 is  $R_{\text{Edd}} = L_{\text{disk}} / L_{\text{Edd}} \sim 0.21$ , where  $L_{\text{Edd}}$  is the Eddington luminosity. We plot  $P_r$  against  $L_{\text{disk}}$  together with their relations in units of Eddington luminosity for CTD 135 and other  $\gamma$ -ray emitting AGNs (the data to see Zhang et al. 2020a), as illustrated in Figure 7. We find that CTD 135, similar to  $\gamma$ -ray emitting CSSs, also obeys the linear regression fit line of other subclasses of  $\gamma$ -ray emitting AGNs in Zhang et al. (2020a), likely implying that its jet radiation is also driven by the Eddington ratio and  $R_{\text{Edd}}$  would be a key physical driver for the unification scheme of AGN jet radiation.

### 4.2 an Aligned Jet and the Symmetric Radio Structure of CTD 135

Different from other  $\gamma$ -ray emitting CSOs and CSSs (Müller et al. 2014; Migliori et al. 2016; Principe et al. 2020; Lister et al. 2020; Zhang et al. 2020a), significant variability and high luminosity in  $\gamma$ -ray band are observed for CTD 135 as blazars. The derived variability index is  $\text{TS}_{\text{var}} = 1002$  for CTD 135, which is

421 and  $TS_{\text{var}} = 543$  for Mrk 501 (Abdollahi et al. 2020). It is also interesting that a QPO signature is detected in the  $\gamma$ -ray light curve of CTD 135, which is generally observed in blazars (Sandrinelli et al. 2014, 2017; Ackermann et al. 2015; Yan et al. 2018; Zhou et al. 2018; Zhang et al. 2020b). Generally, the QPO signature is thought to be due to a super-massive black hole binary system (e.g., Sillanpaa et al. 1988; Lehto & Valtonen 1996; Graham et al. 2015). The precession (e.g., Stirling et al. 2003; Caproni et al. 2013) or helical structure (e.g., Conway & Murphy 1993; Villata & Raiteri 1999; Nakamura & Meier 2004; Chen & Zhang 2021) of jets in blazars can also lead to the QPO signal. Sandrinelli et al. (2017) suggested that the QPOs in these jet-dominant sources are likely owing to the instability or structure of a jet and the oscillation is amplified by the Doppler boosting effect. All these  $\gamma$ -ray emission properties favor the idea that the core emission of CTD 135 has significant Doppler boosting effect like a blazar jet.

As described in Section 3, the broadband SED of CTD 135 can be well fitted with the leptonic model by assuming a small viewing angle ( $\theta$ ), being similar to blazars. We assumed  $\delta = \Gamma$  during the SED fitting for CTD 135, i.e., the viewing angle ( $\theta$ ) being equal to the opening angle ( $1/\Gamma$ ) of jet (e.g., Chen & Zhang 2021), and thus it is  $\theta \sim 5.3^\circ$  for  $\delta = \Gamma = 10.8$ . Using the VLBI measurements of the core angular dimension and radio flux and comparing the predicted and observed X-ray flux in the SSC model frame, Ghisellini et al. (1993) estimated the Doppler factor of  $\delta = 5.2$  and then obtained  $\theta < 11.1^\circ$  for CTD 135. Using the flux-density variations at radio band, Lioudakis et al. (2018) inferred the variability Doppler factor of  $\delta_{\text{var}} = 20.19$  and  $\theta < 2.84^\circ$  (corresponding to  $\Gamma \sim 10.38$ ). These estimates are generally consistent with the values of blazar jets and imply a small viewing angle of jet in CTD 135. However, the symmetric radio structure of CSOs is thought to be due to a misaligned jet to the observers (Phillips & Mutel 1980; Wilkinson et al. 1994; Readhead et al. 1996a). We thus propose that the symmetric radio structure of CTD 135 consists of a relativistic jet surrounding by a bubble similar to the Fermi bubbles in the Galaxy (Su et al. 2010). The  $\gamma$ -rays of CTD 135 are dominated by the relativistic jet radiation as blazars and the symmetric radio structure (symmetric lobes on both sides of the core) is attributed to bubbles.

The Fermi bubbles may be created by a recent AGN jet activity (Guo & Mathews 2012) or the remnants of a large-scale wide-angle outflow from the central supermassive black hole (Zubovas et al. 2011). Recently Lister et al. (2020) reported that the lack of compact, inverted spectrum hotspots and an emission gap between the bright inner jet and outer radio lobe structure for  $\gamma$ -ray emitting CSO TXS 0128+554 is due to the episodic jet activity. The episodic jet activity was theoretically suggested for young radio sources (e.g., Reynolds & Begelman 1997; Czerny et al. 2009). We thus speculate that the pc-scale lobes of CTD 135 are remnants from the previous period of jet activity and the observed  $\gamma$ -rays are associated with the inner jet that was launched more recently, similar to TXS 0128+554. And the re-launched jet of CTD 135 has a small viewing angle like blazar jet, which leads to the strong Doppler boosting effect, the significant variability, and the high  $\gamma$ -ray luminosity. Due to the episodic/short-lived jet activity, some weak CSOs like TXS 0128+554 may never grow to large sizes (Lister et al. 2020) while some strong CSOs like CTD 135

## 5 SUMMARY

In this paper, we comprehensively analyzed the  $\sim 11$ -year Fermi/LAT observation data of CTD 135, confirming that it is spatially associated with 4FGL J2236.3+2828. CTD 135 has a high  $\gamma$ -ray luminosity similar to FSRQs. The average spectrum of CTD 135 in the LAT energy band is very curved and needs a LogParabole spectral model to fit. The variability index of  $TS_{\text{var}} = 1002$  for CTD 135 indicates that its  $\gamma$ -ray fluxes are obviously variable. And a QPO signature with a periodicity of  $\sim 460$  days at a confidence level of  $\sim 95\%$  is presented in the  $\gamma$ -ray light curve of CTD 135. The high luminosity and obvious variability as well as the QPO signature in the  $\gamma$ -ray band demonstrate the strong Doppler boosting effect in CTD 135. The strong Doppler boosting effect implies a small viewing angle of the core jet for CTD 135, which is not coincident with its symmetric radio structure. We proposed that an episodic jet exists in the core region of CTD 135. Its pc-scale lobes are remnants from the previous period of jet activity similar to the Fermi bubbles in the Galaxy while its  $\gamma$ -rays originate from a relaunched relativistic jet.

We also constructed the broadband SED of CTD 135 using the derived  $\gamma$ -ray spectrum together with the data from the ASDC and NED. It can be well explained with the two-zone leptonic model and the  $\gamma$ -ray emission with obvious variability should be from the radiations of the core jet. The derived values of  $B$ ,  $\gamma_b$ , and  $\delta$  for the core region are similar to those of blazars. On the base of SED fitting parameters, we calculated  $P_r$ ,  $P_e$ ,  $P_B$ , and  $P_{\text{jet}}^{e\pm}$  of the core region for CTD 135. Similar to  $\gamma$ -ray emitting CSSs, CTD 135 also has the large values of  $P_r/P_{\text{jet}}^{e\pm}$  and  $P_B/P_{\text{jet}}^{e\pm}$ , indicating that its core region may be highly magnetized with high radiation efficiency. We estimated the disk luminosity in CTD 135 with  $L_{\text{disk}} = 10 * L_{\text{BLR}}$ , and then plotted  $P_r$  against  $L_{\text{disk}}$  together with their relation in units of Eddington luminosity. We found that CTD 135 also follows the linear regression fit line of other subclasses of  $\gamma$ -ray emitting AGNs in Zhang et al. (2020a). Hence, we proposed that the jet radiation of CTD 135 is also driven by the Eddington ratio, similar to other  $\gamma$ -ray emitting AGNs.

**Acknowledgements** This work is supported by the National Natural Science Foundation of China (grants 12022305, 11973050, 11863007, U1738136, U1731239, 11851304, and 11533003), and Guangxi Science Foundation (grants 2017AD22006, 2019AC20334, and 2018GXNSFGA281007).



**References**

- Abdollahi, S., Acero, F., Ackermann, M., et al. 2020, *ApJS*, 247, 33
- Achterberg, A., Gallant, Y. A., Kirk, J. G., et al. 2001, *MNRAS*, 328, 393
- Ackermann, M., Ajello, M., Atwood, W. B., et al. 2015, *ApJ*, 810, 14
- An, T., Cui, Y.-Z., Gabányi, K. É., et al. 2016, *Astronomische Nachrichten*, 337, 65
- An, T. & Baan, W. A. 2012, *ApJ*, 760, 77
- Angioni, R., Ros, E., Kadler, M., et al. 2019, *A&A*, 627, A148
- Angioni, R., Ros, E., Kadler, M., et al. 2020, *A&A*, 641, A152
- Begelman, M. C. 1996, *Cygnus A – Studay of a Radio Galaxy*, 209
- Caproni, A., Abraham, Z., & Monteiro, H. 2013, *MNRAS*, 428, 280
- Celotti, A., Padovani, P., & Ghisellini, G. 1997, *MNRAS*, 286, 415
- Chen, L. & Zhang, B. 2021, *ApJ*, 906, 105
- Conway, J. E. & Murphy, D. W. 1993, *ApJ*, 411, 89
- Czerny, B., Siemiginowska, A., Janiuk, A., et al. 2009, *ApJ*, 698, 840
- D’Ammando, F., Orienti, M., Giroletti, M., et al. 2016, *Astronomische Nachrichten*, 337, 59
- de Vries, W. H., Barthel, P. D., & O’Dea, C. P. 1997, *A&A*, 321, 105
- Fanti, C. 2009, *Astronomische Nachrichten*, 330, 120
- Fanti, C., Fanti, R., Dallacasa, D., et al. 1995, *A&A*, 302, 317
- Fassnacht, C. D. & Taylor, G. B. 2001, *AJ*, 122, 1661
- Franceschini, A., Rodighiero, G., & Vaccari, M. 2008, *A&A*, 487, 837
- Ghisellini, G., Padovani, P., Celotti, A., et al. 1993, *ApJ*, 407, 65
- Ghisellini, G. & Tavecchio, F. 2009, *MNRAS*, 397, 985
- Graham, M. J., Djorgovski, S. G., Stern, D., et al. 2015, *Nature*, 518, 74
- Gugliucci, N. E., Taylor, G. B., Peck, A. B., et al. 2005, *ApJ*, 622, 136
- Guo, F., Liu, Y.-H., Daughton, W., et al. 2015, *ApJ*, 806, 167
- Guo, F. & Mathews, W. G. 2012, *ApJ*, 756, 181
- Hovatta, T., Valtaoja, E., Tornikoski, M., et al. 2009, *A&A*, 494, 527
- Johnston, K. J., Fey, A. L., Zacharias, N., et al. 1995, *AJ*, 110, 880
- Kino, M., Kawakatu, N., & Ito, H. 2007, *MNRAS*, 376, 1630
- Kino, M., Ito, H., Kawakatu, N., et al. 2009, *MNRAS*, 395, L43
- Kino, M. & Asano, K. 2011, *MNRAS*, 412, L20
- Kirk, J. G., Guthmann, A. W., Gallant, Y. A., et al. 2000, *ApJ*, 542, 235
- Lehto, H. J. & Valtonen, M. J. 1996, *ApJ*, 460, 207
- Liodakis, I., Hovatta, T., Huppenkothen, D., et al. 2018, *ApJ*, 866, 137
- Lister, M. L., Homan, D. C., Kovalev, Y. Y., et al. 2020, *ApJ*, 899, 141
- Lomb, N. R. 1976, *Ap&SS*, 39, 447
- Massaro, E., Perri, M., Giommi, P., et al. 2004, *A&A*, 413, 489
- Mattox, J. R., Bertsch, D. L., Chiang, J., et al. 1996, *ApJ*, 461, 396
- Migliori, G., Siemiginowska, A., Kelly, B. C., et al. 2014, *ApJ*, 780, 165

- Migliori, G., Siemiginowska, A., Sobolewska, M., et al. 2016, *ApJ*, 821, L31
- Murgia, M. 2003, *PASA*, 20, 19
- Murphy, D. W., Browne, I. W. A., & Perley, R. A. 1993, *MNRAS*, 264, 298
- Müller, C., Krauß, F., Dauser, T., et al. 2015, *A&A*, 574, A117
- Müller, C., Kadler, M., Ojha, R., et al. 2014, *A&A*, 562, A4
- Nakamura, M. & Meier, D. L. 2004, *ApJ*, 617, 123
- Nolan, P. L., Abdo, A. A., Ackermann, M., et al. 2012, *ApJS*, 199, 31
- O’Dea, C. P. 1998, *PASP*, 110, 493
- O’Dea, C. P. & Baum, S. A. 1997, *AJ*, 113, 148
- Orienti, M., Dallacasa, D., Tinti, S., et al. 2006, *A&A*, 450, 959
- Peck, A. B. & Taylor, G. B. 2000, *ApJ*, 534, 90
- Peng, F.-K., Zhang, H.-M., Wang, X.-Y., et al. 2019, *ApJ*, 884, 91
- Phillips, R. B. & Mutel, R. L. 1980, *ApJ*, 236, 89
- Phillips, R. B. & Mutel, R. L. 1982, *A&A*, 106, 21
- Principe, G., Migliori, G., Johnson, T. J., et al. 2020, *A&A*, 635, A185
- Readhead, A. C. S., Taylor, G. B., Pearson, T. J., et al. 1996a, *ApJ*, 460, 634
- Readhead, A. C. S., Taylor, G. B., Xu, W., et al. 1996b, *ApJ*, 460, 612
- Reynolds, C. S. & Begelman, M. C. 1997, *ApJ*, 487, L135
- Sandrinelli, A., Covino, S., & Treves, A. 2014, *ApJ*, 793, L1
- Sandrinelli, A., Covino, S., Treves, A., et al. 2017, *A&A*, 600, A132
- Scargle, J. D. 1982, *ApJ*, 263, 835
- Schmidt, M. 1977, *ApJ*, 217, 358
- Shaw, M. S., Romani, R. W., Cotter, G., et al. 2012, *ApJ*, 748, 49
- Sillanpaa, A., Haarala, S., Valtonen, M. J., et al. 1988, *ApJ*, 325, 628
- Sironi, L. & Spitkovsky, A. 2014, *ApJ*, 783, L21
- Stanghellini, C., O’Dea, C. P., Dallacasa, D., et al. 1998, *A&AS*, 131, 303
- Stawarz, Ł., Ostorero, L., Begelman, M. C., et al. 2008, *ApJ*, 680, 911
- Stirling, A. M., Cawthorne, T. V., Stevens, J. A., et al. 2003, *MNRAS*, 341, 405
- Su, M., Slatyer, T. R., & Finkbeiner, D. P. 2010, *ApJ*, 724, 1044
- Sun, X.-N., Zhang, J., Lin, D.-B., et al. 2015, *ApJ*, 798, 43
- van Breugel, W., Miley, G., & Heckman, T. 1984, *AJ*, 89, 5
- Villata, M. & Raiteri, C. M. 1999, *A&A*, 347, 30
- Virtanen, J. J. P. & Vainio, R. 2005, *ApJ*, 621, 313
- Wilkinson, P. N., Polatidis, A. G., Readhead, A. C. S., et al. 1994, *ApJ*, 432, L87
- Xi, S.-Q., Zhang, H.-M., Liu, R.-Y., et al. 2020, *ApJ*, 901, 158
- Yan, D., Zhou, J., Zhang, P., et al. 2018, *ApJ*, 867, 53
- Zenitani, S. & Hoshino, M. 2001, *ApJ*, 562, L63
- Zhang, J., Liang, E.-W., Zhang, S.-N., et al. 2012, *ApJ*, 752, 157
- Zhang, J., Sun, X.-N., Liang, E.-W., et al. 2014, *ApJ*, 788, 104

- Zhang, J., Xue, Z.-W., He, J.-J., et al. 2015, *ApJ*, 807, 51
- Zhang, J., Zhang, H.-M., Zhu, Y.-K., et al. 2017, *ApJ*, 849, 42
- Zhang, J., Zhang, H.-M., Gan, Y.-Y., et al. 2020, *ApJ*, 899, 2
- Zhou, J., Wang, Z., Chen, L., et al. 2018, *Nature Communications*, 9, 4599
- Zhang, P.-fei., Yan, D.-hai., Zhou, J.-neng., et al. 2020, *ApJ*, 891, 163
- Zhu, Y.-K., Zhang, J., Zhang, H.-M., et al. 2016, *Research in Astronomy and Astrophysics*, 16, 170
- Zubovas, K., King, A. R., & Nayakshin, S. 2011, *MNRAS*, 415, L21

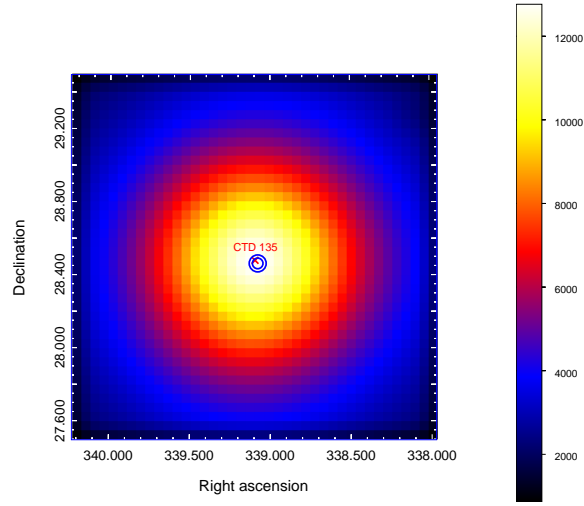


**Fig. 1**  $2^\circ \times 2^\circ$  TS map of CTD 135. The red cross represents the radio position of CTD 135. The blue contours represent the 68% and 95% confidence levels of the gtfndsrc best-fit position with the  $\sim 11$ -year Fermi/LAT observation data. The map is created with a pixel size of  $0.05^\circ$ .

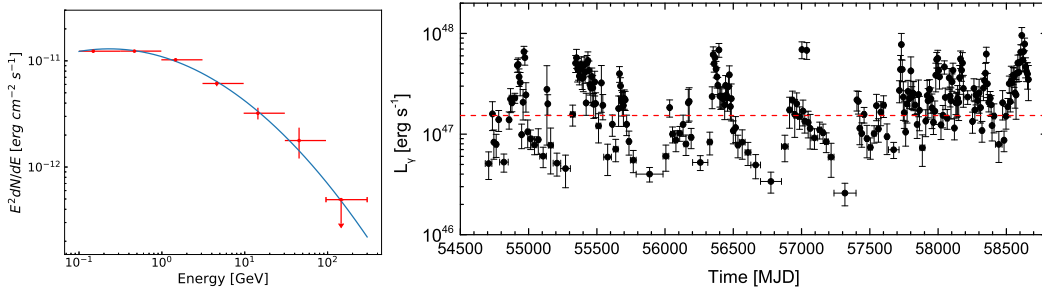


**Fig. 2** Left panel: the  $\sim 11$ -year average spectrum of CTD 135 observed by Fermi/LAT in energy band of 0.1–300 GeV. The blue solid line represents the fitting result with a LogParabole spectral model. Right panel: long-term light curve observed by Fermi/LAT for CTD 135, where a adaptive-binning method based on the constraint of  $\text{TS} = 25$  is used, i.e., the detections of all data points being larger than  $5\sigma$ . The red horizontal dashed line represents the  $\sim 11$ -year average luminosity of CTD 135.

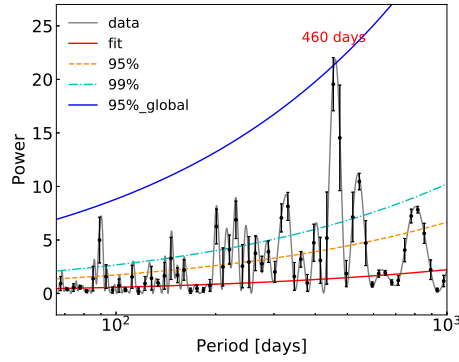


**Fig. 3** LSP of  $\gamma$ -ray light curve is marked as gray line. The black points with corresponding errors indicate the re-binned data of LSP. The best-fit power spectrum is shown as red solid line. The orange dash line and cyan dot-dashed line represent the single-frequency 95% and 99% confidence level lines, respectively. The blue solid line represents the global 95% false-alarm level of the power-law model.

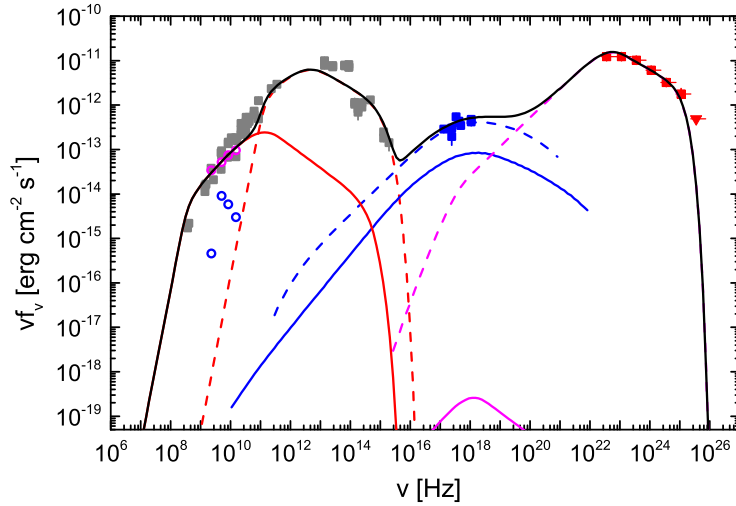


**Fig. 4** Observed SED with the two-zone leptonic radiation model fitting. The gray squares are taken from the NED, the blue squares are taken from the ASDC, and the red squares are the average spectrum of the Fermi/LAT observations. The magenta and blue opened circles indicate the fluxes from component-NE+core and component-SW (taken from An et al. 2016), respectively. The black solid line indicates the total emission of the two regions. The colored solid and dashed lines represent the radiations from the extended region and the core region, respectively; red lines for synchrotron, blue lines for SSC, magenta lines for EC.

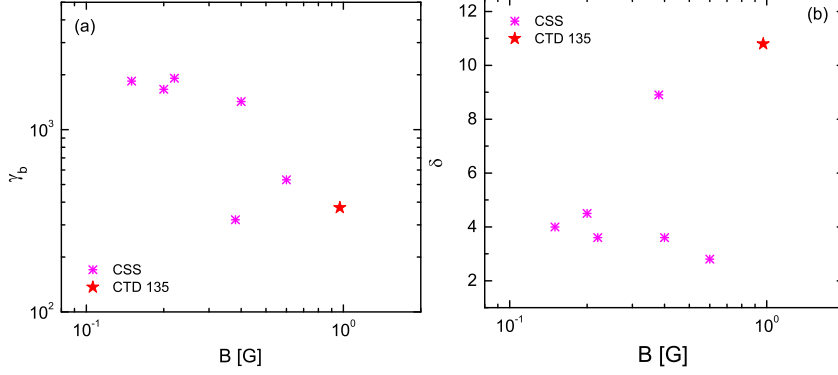


**Fig. 5**  $\gamma_b$  and  $\delta$  as a function of  $B$ . The data of six  $\gamma$ -ray emitting CSSs are taken from Zhang et al. (2020a).

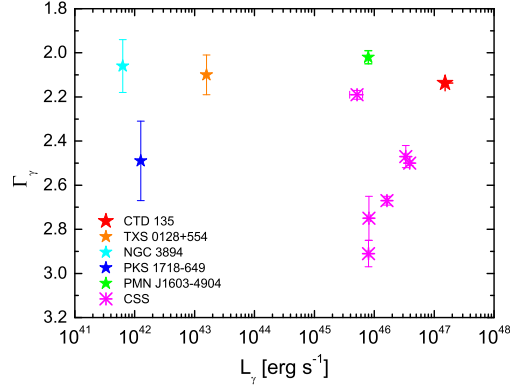


**Fig. 6**  $\Gamma_\gamma$  against  $L_\gamma$ , where  $\Gamma_\gamma$  and  $L_\gamma$  of CTD 135 are the  $\sim 11$ -year average photon spectral index and  $\gamma$ -ray luminosity, respectively, observed by Fermi/LAT. The data of six  $\gamma$ -ray emitting CSSs and other four  $\gamma$ -ray emitting CSOs are taken from Zhang et al. (2020a) and Abdollahi et al. (2020), respectively.

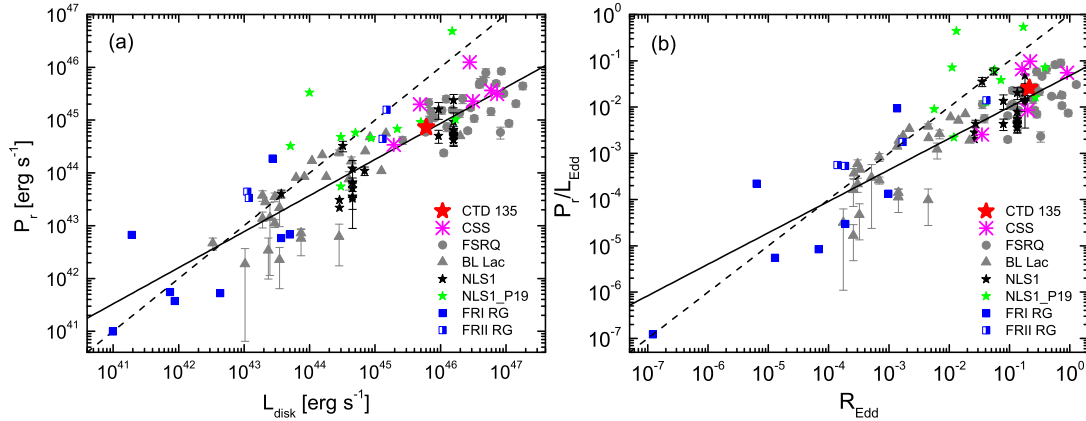


**Fig. 7**  $P_r$  as a function of  $L_{\text{disk}}$  together with their relations in units of Eddington luminosity for CTD 135. The dashed lines indicate the equality line while the solid lines are the linear regression fits for other detected  $\gamma$ -ray emitting AGNs (including blazars, NLS1s, radio galaxies, and CSSs, taken from Zhang et al. 2020a).